Heat Flux Measurements in High Enthalpy Flows

A. Gülhan
German Aerospace Center (DLR)
Institute of Fluid Mechanics
Wind Tunnel Division in Cologne
Porz-Wahnheide, Linder Höhe
D-51147 Cologne, Germany

Summary

This document describes the fundamentals of heat transfer measurement techniques in high enthalpy flows. After description of basic relations for the stagnation point heat flux rate to a spherical surface in a high enthalpy flow field, different heat flux measurement techniques are discussed. Attention is paid to design aspects, mathematical model for the heat flux rate evaluation and application limits of each sensor type, in order to provide a useful and practical script for the reader with respect to the choice of an adequate sensor type for different requirements. Sensor calibration and comparative measurements using different heat flux sensors in the arc heated facility LBK are described in the last two chapters.

1. List of symbols

A	cross section area
C_p	specific heat
D_{12}	binary diffusion coefficient for atoms and molecules
h	enthalpy
h_D	enthalpy of dissociation per unit mass for the gas in the external flow
K	thermal conductivity
LBK	arc heated facility of DLR
Le	Lewis number
$\dot{m}$	mass flow rate
Nu	Nusselt number
p	pressure
Pr	Prandtl number
$\dot{q}$	heat flux rate
Re	Reynolds number
s	wall thickness
T	temperature
u	flow velocity component in the direction parallel to the body surface
ε	emissivity
ρ	density

Subscripts

c	coolant
e	boundary layer edge
s	stagnation point
w	wall
0	stagnation condition
1	inlet side
2	outlet side
∞	ambient, free stream

2. Introduction

Intrusive measurement techniques in supersonic and hypersonic flows have been a challenging task for engineers for decades. Recent progresses in non-intrusive measurement techniques and numerical codes have led to a better understanding of local flow phenomena and to further improvement of intrusive measurement techniques in aerodynamics. Because of its complexity the measurement of the

Paper presented at the RTO AVT Course on "Measurement Techniques for High Enthalpy and Plasma Flows", held in Rhode-Saint-Genèse, Belgium, 25-29 October 1999, and published in RTO EN-8.

heat flux rate remains one of the key techniques, which have to be improved with respect to measurement accuracy and repeatability. The heat flux rate is usually determined from the measured temperature development on the surface or inside the probe and applying a mathematical model with some assumptions. Any deviation from a perfect contact between the temperature sensor and probe or other satisfaction of assumptions leads to inaccuracies.

Heat flux determination in high enthalpy flow fields is accompanied with some additional effects. Since the flow field of most of the high enthalpy facilities is in thermo-chemical non-equilibrium, the gas surface interaction phenomena influence the heat flux rate significantly. Surface catalysis and emittance, which are a function of the surface temperature, play an important role in such environments. The boundary flow around the probe is also influenced by these effects and there is a continuous coupling between the flow and model structure. Differences in the operation of different high enthalpy facilities give rise to different requirements on the heat flux sensors. Short duration high enthalpy facilities like shock tunnels, impulse facilities, etc. have a very short testing time of several milliseconds. Therefore only heat flux sensors with a very short response time can be used in these facilities. Because of short flow exposure time of the sensor the surface temperature is low. Arc heated and induction heated facilities have a longer testing time, which would lead to higher surface temperature of the stationary and uncooled probes. The practical realisation of the cooling and insulation of the probe influences the measurement. Another option is the application of uncooled transient heat flux probes, whose reliability depend on some further parameters like sweep speed, flow homogeneity, etc..

Because of above mentioned diversity in the requirement on heat flux sensors different types of measurement techniques will be described and compared in this document. Since some techniques can be used in both short and long test duration facilities, the layout of this script is chosen in such a way that similar techniques are described in the same chapter.

3. Heat flux at high surface temperatures

The heat transfer process at hypersonic velocities is complicated by high temperature effects, which are not present at low speed flights. The shock wave in front of the critical components of a hypersonic vehicle like nose cap, wing leading edge, etc. heats air to high temperatures at which dissociation and ionization of the gas species take place (**Fig. 1**).

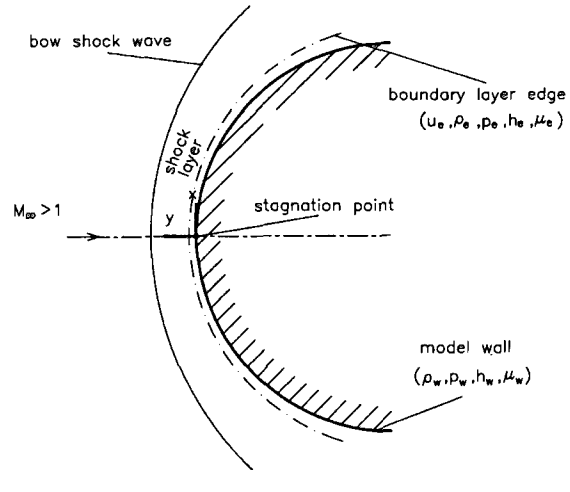

Figure 1. Stagnation region flow field

Since the dissociation and ionization processes proceed at finite rates and the relaxation length behind a bow shock is small the thermochemical

equilibrium is not necessarily be achieved in the stagnation point region. Depending on the shock strength, i.e. flight Mach number, the gas at the boundary layer edge consists of different composition of molecules, atoms and ions. The vibrational rotational and translational excitations of molecules are not in equilibrium. Due to viscous forces in the boundary layer the gas is decelerated and recombination reactions are initiated. Since atoms and ions recombine with a high specific energy release the heat transfer rate is enhanced. If a fully thermochemical equilibrium of the gas is not achieved in the boundary layer, the heat flux rate to the body depends on the catalysis of the surface.

The stagnation point heat transfer rate to a spherical body in a dissociated viscous boundary flow with thermochemical equilibrium was described by Fay and Riddell [1,2] as follows:

$$\dot{q}_s = 0.76\, Pr^{-0.6}(\rho_e\mu_e)^{0.4}\,(\rho_w\mu_w)^{0.1}\sqrt{\left(\frac{du_e}{dx}\right)_s}\,(h_{0_e}-h_w)\left[1+\left(Le^{0.52}-1\right)\left(\frac{h_D}{h_{0_e}}\right)\right] \quad (1)$$

The non-dimensional parameters appearing in this formula are defined as

Prandtl number

$$Pr = \frac{\mu C_p}{K} \quad (2)$$

Lewis number

$$Le = \frac{\rho C_p D_{12}}{K}. \quad (3)$$

The other notations used in the equation (1) are

C_p: specific heat

D_{12}: binary diffusion coefficient for atoms and molecules

h: enthalpy

h_D: enthalpy of dissociation per unit mass for the gas in the external flow

K: thermal conductivity

$\dot{q}_s$: stagnation point heat flux rate

u: flow velocity component in the direction parallel to the body surface

x: radial distance along the body surface from the stagnation point

μ: viscosity

ρ: density

The subscript notation is:

0: conditions at the stagnation point

e: conditions at the boundary layer edge

w: conditions at the body surface

The stagnation point velocity gradient is given by Newtonian theory as:

$$\left(\frac{du_e}{dx}\right)_s = \frac{1}{R}\sqrt{\frac{2(p_e-p_\infty)}{\rho_e}} \quad (4)$$

where R is the radius of the sphere, p_e and p_∞ are the pressure at the stagnation point of the boundary layer edge and the pressure ahead of the shock, respectively.

The heat flux rate of a fully catalytic spherical wall in a frozen boundary layer is given as

$$\dot{q}_s = 0.76\, Pr^{-0.6}(\rho_e\mu_e)^{0.4}\,(\rho_w\mu_w)^{0.1}\sqrt{\left(\frac{du_e}{dx}\right)_s}\,(h_{0_e}-h_w)\left[1+\left(Le^{0.63}-1\right)\left(\frac{h_D}{h_{0_e}}\right)\right] \quad (5)$$

The heat flux rate to a non-catalytic surface in a frozen boundary layer is approximated with $Le = 0$ as:

$$\dot{q}_s = 0.76\, Pr^{-0.6}(\rho_e\mu_e)^{0.4}\,(\rho_w\mu_w)^{0.1}\sqrt{\left(\frac{du_e}{dx}\right)_s}\left(1-\frac{h_D}{h_{0_e}}\right). \quad (6)$$

The equations (1) and (5) describing the heat flux rate to an arbitrary surface in an equilibrium flow and the heat flux rate to a fully catalytic surface in a frozen flow field, respectively, are essentially the same. They differ only in the slightly different exponent on the Lewis number. That means that the surface heat flux rate is nearly the same whether the flow is in local thermochemical equilibrium or is frozen with a fully catalytic wall. In the case of an equilibrium flow recombination reaction takes place in the colder region of the boundary layer itself, releasing chemical energy, which is transported by thermal conductance to the surface. In the frozen boundary layer flow recombination occurs on the catalytic wall surface. **Figure 2** shows the heat transfer coefficient $Nu/\sqrt{Re}$ as a function of the recombination rate parameter C_1 [3]. Nusselt number (Nu), Reynolds number (Re) and C_1 are defined as:

$$Nu = \frac{\dot{q}_s C_{p_w} x}{K_w(h_e - h_w)} \quad (7)$$

$$Re = \frac{\rho_w u_e x}{\mu_w} \quad (8)$$

$$C_1 = K_1 p_s^2 T_s^{-3.5} R^{-2}\left(\frac{du_e}{dx}\right)_s^{-1}. \quad (9)$$

R is the universal gas constant.

The solid lines show the total heat flux rate for both catalytic (1) and non-catalytic (2) surfaces. The heat flux rate by conduction alone to a catalytic wall is shown by the dotted curve (3). Large values of C_1 corresponds to an equilibrium boundary layer flow. At this range the total heat transfer is dominated by conductive heating. As mentioned before in an equilibrium flow the heat flux rate to both catalytic and non-catalytic surfaces is the same since the recombination is completed in the boundary layer flow. In contrast the heat flux rate to a non-catalytic wall depends strongly on the flow regime. By moving from high C_1 values (equilibrium) to smaller C_1 values the flow becomes progressively more non-equilibrium and it is frozen at the left end of the curves. It can be seen clearly that the heat flux rate to a non-catalytic wall (curve 2) in the frozen flow field drops by a factor of more than two compared to the equilibrium flow. The difference between the curves 1 and 3 represents the heat transfer due to diffusion. It can be seen clearly that at decreasing C_1, i.e. freezing boundary layer chemistry, the conductive heat transfer rate to the wall is decreasing. Although for equilibrium flows the total heat transfer is essentially all conductive, the diffusion becomes a larger part of the heat transfer to a catalytic wall in strong non-equilibrium flow.

The influence of the non-equilibrium phenomena in the gas-surface-interaction in high enthalpy flow field has to be considered in the measurement techniques of the heat flux rate determination in high enthalpy facilities.

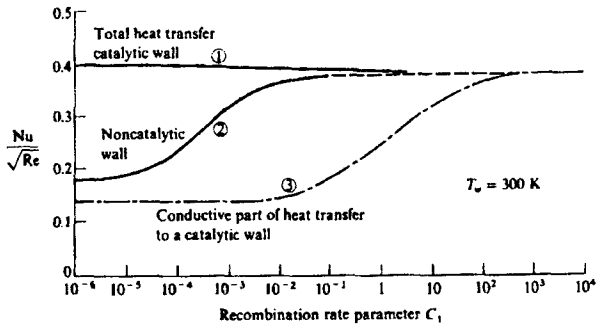

Figure 2. Heat transfer parameter C_1 for different wall catalysis [1,2]

4. Heat flux measurement techniques

Fay and Riddell equation for the stagnation point heat flux rate does not include radiation effects. Since the radiance of a surface is a strong function of the surface temperature and its development depends also on the thermal properties of the vehicle or model materials, it has to be considered by the analysis of heat balance of a solid surface. Although especially in high density gas with high temperature, radiation processes may affect the heat transfer from the gas to the model significantly, thermal radiation of the surface at high temperatures is more important. Therefore thermal radiance of the surface is considered in the analysis of the heat balance on the model surface.

Let us consider a test model, which is exposed to a high enthalpy flow field (**Fig. 3**).

The heat balance on the model surface can be expressed as

$$\dot{q}_g = \dot{q}_c + \dot{q}_r \tag{10}$$

where $\dot{q}_g$, $\dot{q}_c$ and $\dot{q}_r$ represent the heat flux rate from the gas to the surface, conduction inside the model and thermal radiation of the model surface, respectively. The thermal radiance is a strong function of the surface temperature

$$\dot{q}_r = \varepsilon\sigma\left(T_w^4 - T_\infty^4\right) \tag{11}$$

where ε and σ (= $5.67 \cdot 10^{-8}$ [W/(m^2 · K^{-4})]) are the surface emissivity and the Stefan-Boltzmann constant, respectively.

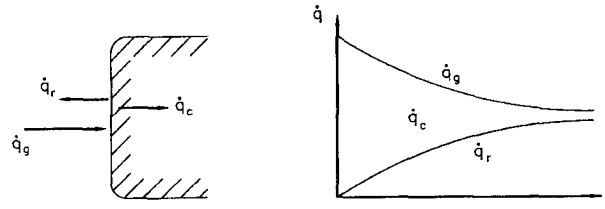

Figure 3. Heat transfer balance at the model wall

At low temperatures of the model in a high enthalpy flow field the thermal radiance ($\dot{q}_r$) is negligible compared to the gas heating (Fig. 3). Since the difference of the gas and surface temperatures is a driving factor of the heat transfer from the gas surface to the model surface (eqs. (1), (2) and (3)), it is high at cold surfaces in a high temperature gas flow. Therefore the heat conduction into the model, i.e. temperature increase in the model structure, is high. Since the gas heating to the surface and radiation cooling of the model have an opposite development with increasing temperature, a so-called radiative equilibrium establishes at high surface

temperatures. At that point the gas heating rate and radiation cooling rate are equal. The heat flux rate to a surface in radiative equilibrium can be determined by measuring the surface temperature and applying the equation (11). The surface temperature can be measured with non-intrusive measurement techniques like pyrometer or IR-camera. Besides an accurate temperature measurement a correct value of the surface emissivity ε is essential for the determination of the so-called hot wall heat flux rate. This technique can only be applied in arc heated or induction heated facilities with long testing time (several minutes), where radiative equilibrium can be achieved.

In order to determine the heat flux rate to models without radiative equilibrium conditions which are achieved in long duration high enthalpy facilities, shock tunnels or hot shot facilities use different measurement techniques.

4.1 Heat storage and conduction sensors

4.1.1 Transient heat flux probe of DLR

The transient heat flux probe designed by DLR [4] consists of a copper cylinder with two embedded thermocouples at both ends of the cylinder (**Fig. 4**). It is integrated in a water cooled probe holder almost adiabatically.

The probe is swept through the flow field at constant flow conditions. Since the probe temperature is mostly lower than 500 K and copper surface is catalytic, this probe provides cold wall heat flux rate to a catalytic surface. The heat flux rate is determined from measured temperature development at two locations and applying one dimensional heat conduction equation. The measured temperature developments are the boundary conditions of this equation.

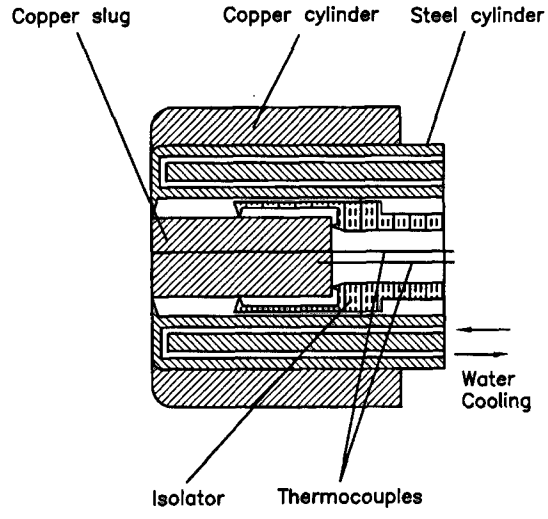

Figure 4. Transient heat flux probe of DLR

Based on the description in the **Fig. 5** the heat conduction equation can be written as below:

$$\frac{\partial T}{\partial t} = \frac{K}{\rho C_p} \frac{\partial^2 T}{\partial x^2} \tag{12}$$

where T, t and x are the temperature, the time and the axial distance from the front of probe surface. The parameters K, ρ and C_p represents the thermal conductivity, the density and the specific heat of the copper cylinder, respectively.

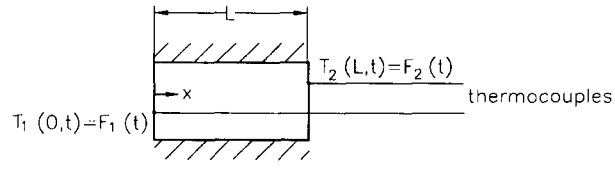

Figure 5. Mathematical model of the transient heat flux probe

The initial condition is

$$T(x,0) = T_0 . \tag{13}$$

The boundary conditions are given by two functions $F_1(t)$ and $F_2(t)$:

$$T(0,t) = F_1(t) \tag{14}$$

$$T(L,t) = F_2(t) \tag{15}$$

where L is the length of the cylinder.

Since the solution of the equation (12) requires complicated Laplace transformations, it is not described here in details. Using the determined temperature development along the cylinder by solving equation (12), the heat flux rate to the front surface of the probe can be calculated from equation:

$$\dot{q}(0,t) = K\left(\frac{\partial T}{\partial x}\right)_{x=0} . \tag{16}$$

Transient heat flux measurement technique assumes that no heat is lost by conduction in radial direction and thermocouple wires. The first assumption is generally justified by keeping the contact surface of the probe to the probe holder as small as possible (three points around the circumference of the cylinder and use of an insulation material as interface surface). Since the heat conductivity of copper is nearly four times higher than that of Nickel or Chromium (NiCr-Ni thermocouples are used) [5] and the cross section area of thermocouples is very small compared the cylinder surface area the heat sink effect of thermocouples is small. The main uncertainty of this technique is correlated to the quality of vacuum brazing of thermocouples into the copper cylinder. Even small cavities at the measurement spot of thermocouples in the cylinder can influence the accuracy of the probe remarkably. Therefore all braze spots have to be analysed using X-ray before the calibration and use of the probe. The temperature dependency of the material properties (ρ, C_p, K) is considered to achieve a good accuracy of the measurement. This technique also allows to measure the spatial distribution of the heat flux rate.

4.1.2 Heat flux sensor of NAL

National Aerospace Laboratory (NAL) in Tokyo has developed a heat flux sensor for high temperature application using tile material [6]. This sensor was successfully applied during the flight of the HYFLEX vehicle in 1996 [7]. It consists of tile material with a high temperature coating of 0.3 mm thickness (**Fig. 6**). The sensor is attached to the substructure of the vehicle via an aluminium flange and screws.

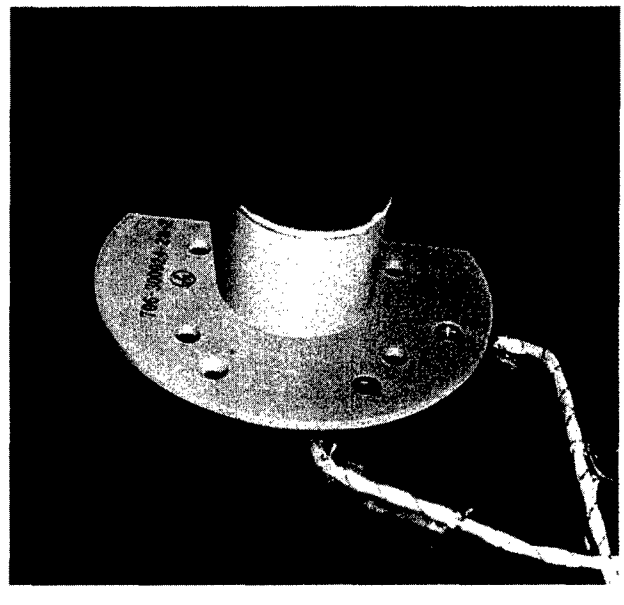

Figure 6. NAL heat flux sensor [6]

Three thermocouples are integrated in the sensor to measure the temperature history at three locations along the axis of the plug (**Fig. 7**). The first thermocouple is attached to the rear surface of the high temperature glass coating layer. The measured temperature is assumed to be the surface temperature of the sensor. The much higher thermal conductivity of the glass coating compared to the ceramic tile justifies this assumption. Using measured temperatures with three thermocouples as boundary conditions under the assumption of two dimensional plane symmetry and applying two dimensional heat conduction equation the heat flux rate is calculated.

NAL sensor is one of the few sensors, which can be used at high temperatures up to 1700 K for flight experiments. It has a response time of about one second. Since it is made of tile materials of the vehicle, the transferability of the data to the thermal behaviour of other TPS components of the vehicle is more reliable compared to sensors consisting of metallic materials. Even the complex data reduction of this sensor does not influence its advantages for flight application.

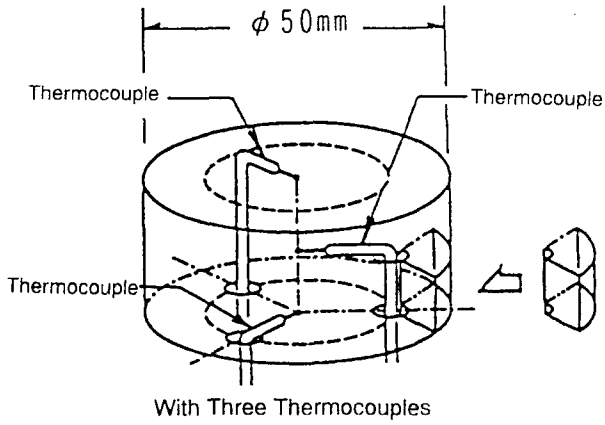

Figure 7. Principle sketch of NAL heat flux sensor [7]

4.2 Sensors based on thick wall technique

The principle of thick wall heat flux sensors is based on the measurement of the surface temperature of a model structure, which can be considered to be a semi-infinite solid (**Fig. 8**). It means that during the measurement time period the conductive heating does not reach the rear surface of the model, i.e. the surface temperature at that location remains constant.

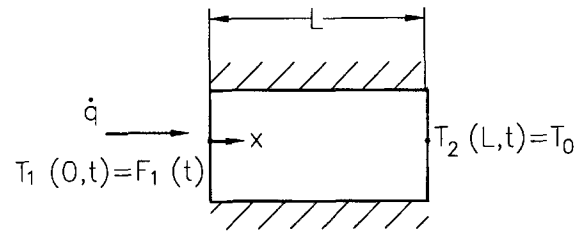

Figure 8. Boundary temperatures of a semi-infinite model

The boundary conditions for the one-dimensional heat conduction equation (eq. (12)) would be:

$$T(0,t) = F_1(t) = T(t) \tag{17}$$

$$\dot{q}_s(t) = K\left(\frac{\partial F_1(t)}{\partial x}\right)_{x=0} = K\left(\frac{\partial T(t)}{\partial x}\right)_{x=0} \tag{17'}$$

$$T(L,t) = T(\infty,t) = T_0. \tag{18}$$

The solution of the equation (12) under these boundary conditions leads to the following expression for the heat flux rate to a semi-infinite probe:

$$\dot{q}(t) = \sqrt{\frac{\rho C_p K}{\pi}}\left[\frac{T(t)}{\sqrt{t}} + \frac{1}{2}\int_0^t \frac{T(t)-T(\tau)}{(t-\tau)^{3/2}}d\tau\right] \tag{19}$$

In the case of a constant heat flux rate equation (19) takes a simpler form:

$$\dot{q} = \frac{\sqrt{\pi}}{2}\sqrt{\frac{\rho C_p K}{t}}\,[T(0,t) - T_0]. \qquad (20)$$

This technique requires a short exposure time of the sensor to the flow. The duration is defined by the constancy of the rear surface temperature of the slug. Therefore it is mainly used in shock tunnels, impulse tunnels or hot shot facilities. The transition phase of the flow after the start makes the heat flux evaluation in these facilities difficult.

4.2.1 Coaxial surface thermocouple

The principal of the application of the coaxial surface thermocouple for the heat flux rate measurement is the measurement of the surface temperature of a body, which can be considered as a semi-infinite solid. One thermoelectric material is installed in a second tube of thermoelectric material concentrically with an electrical insulation of ceramic base (**Fig. 9**). The hot junction of the thermocouple is created by abrading the center conductor and outer tube together. The coaxial thermocouple assembly is completed by attaching thermocouple lead wires to the coaxial thermoelements.

The heat flux rate is determined from the measured surface temperature history by solving equation (19) or (20) using a numerical integration technique.

In order to achieve a representative heat flux rate to the model surface, the material properties of the thermocouple (i.e. $\sqrt{\rho C_p K}$ value) has to match with the model parameters. This technique is applied in short duration wind tunnels, continuous wind tunnels and arc jet facilities. The main advantages of the coaxial thermocouple technique are its fast response time (~ 50 µs) and very good durability. Since the output is self-generating, no calibration is required. It's application is restricted more or less to metal models. Weak output signal and complex data reduction are the disadvantages of this technique.

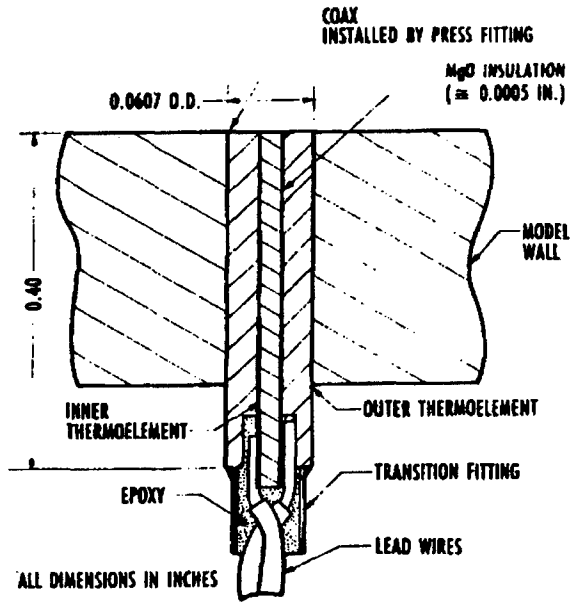

Figure 9. Sketch of coaxial surface thermocouple [8]

Based on already available coaxial thermocouples, a coaxial thermocouple with integrated pressure gauge has been developed at the Technical University of Aachen (RWTH Aachen) (**Fig. 10**) [9]. It allows to measure the temperature, i.e. heat flux rate, and pressure almost at the same location (spatial deviation between two sensors is about 1.5 mm). The sensor properties are matched for its application in short duration facilities.

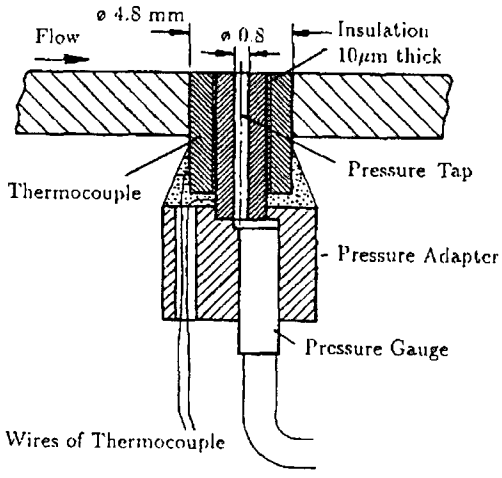

Figure 10. Coaxial surface thermocouple with integrated pressure gauge [9]

4.2.2 Thin-film gauge

Thin film gauges have been extensively used in the aerodynamic research for decades. Mainly a platinum film is applied in a thickness of several nanometers on the substrate by sputtering, vacuum deposition or painting. Pyrex, fused Quarts or MACOR are mainly used as substrate. Because of its high positive temperature-resistance coefficient Platinum provides an excellent output signal. The temperature data deduced from the measured resistance change is reduced to the heat flux rate using semi-infinite heat flux equation (eq. (19) or (20)). **Figure 11** shows a thin film gauge developed at RWTH Aachen [10]. Thin film gauges are very convenient for aerothermodynamic application, since they have a negligible heat capacity compared to the substrate. In contrast to coaxial surface thermocouples thin film gauges find a broad application on non-metallic materials. The other remarkable advantage is their easy use in surface curvatures of small radius. The response time is very short (less than 5 μs). But these sensors are very sensitive even to small particles. The calibration is time consuming. The influence of the heat conduction on the results has to be considered in the evaluation of the data.

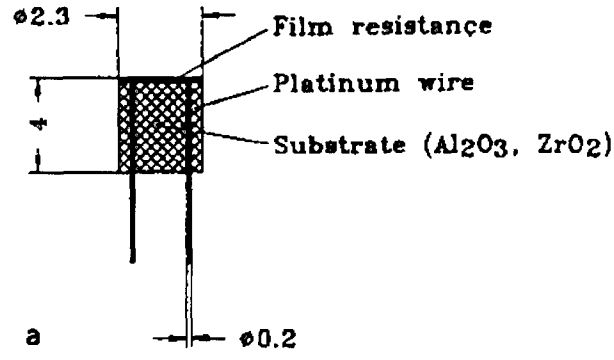

Figure 11. Thin film gauge of RWTH Aachen [10]

4.2.3 Null-point calorimeter

The null-point calorimeter was developed by AEDC [8]. **Figure 12** shows a sketch of this sensor. A thermal mass with a length of several centimetres is drilled from the backside to a few millimetre distance from the front surface.

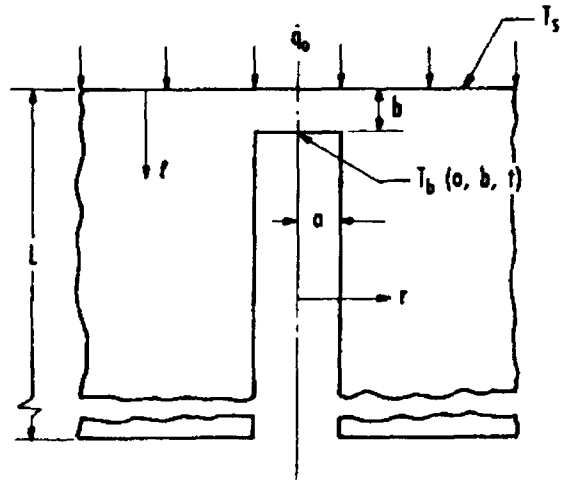

Figure 12. Concept of null-point calorimeter [8]

The location 0, *b* on the radial centerline of the cylinder cavity is defined as the null point. The

measured temperature development of this point is assumed to be identical to the surface temperature history on the outside surface of the same thermal mass without cavity. In order to justify this assumption the geometry of the sensor is specified by a very detailed thermal analysis. According to null point, analysis states that the temperature history at the null point would be very close to the surface temperature history in the absence of the hole, if the ratio of the hole radius to the axial distance of the point about 1.4. Therefore, the measured null point temperature with a Chromel-Alumel thermocouple can be inserted into the equation (19) to determine the heat flux rate to a semi-infinite mass. The thermocouple wires are normally attached by vacuum brazing. As it is shown in **Fig. 13** the null-point body has a slight chamber at the top and bottom, which creates an effective circumferential dead air space along the length of the cylinder to enhance one-dimensional heat conduction and prevent radial heat transfer.

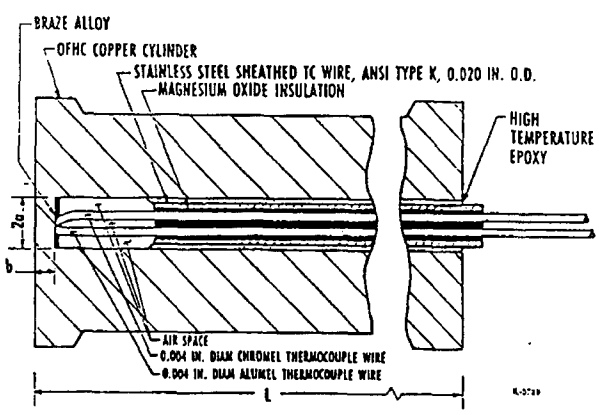

Figure 13. Cross section view of null-point calorimeter [8]

This sensor is mainly used at the stagnation point test configuration of arc heated facilities. Its response time is 1-2 ms. Very high heat flux rates up to 284 MW/m^2 can be measured with this sensor. Shortcomings of the null-point calorimeter are the difficulty in the achievement of consistency in thermocouple wire attachment, difficult calibration procedure and its limitation to high heat flux rates at short time duration.

4.3 Calorimetric sensors

4.3.1 Thin-skin technique

The operation principle of the thin-skin technique involves measuring the slope of the back surface temperature history of a thin skin model.

The heat flux rate can be calculated using the relation:

$$\dot{q} = \rho C_p s \frac{dT}{dt} \tag{21}$$

where s is the thickness of the thin wall.

This technique assumes that the heat conduction to adjacent structures is negligible during the measuring time. The exposure time of the sensor has to be specified in dependence on the material properties and heat flux rate level, i.e. temperature gradient on the back surface. Simple data reduction is a big advantage of this technique. But the influence of the lateral heat conduction and temperature dependency of the material properties on the measurement accuracy is a problem. Therefore the fabrication of a thin-skin model is expensive.

4.3.2 Slug calorimeter

The slug calorimeter technique is based on the storage of all the heat which enters upon the sensor surface in a calorimetric mass during the measuring

time. A metallic disc is mostly used as calorimetric mass. The slug is integrated in a thermal insulator to avoid radial heat losses (**Fig. 14**).

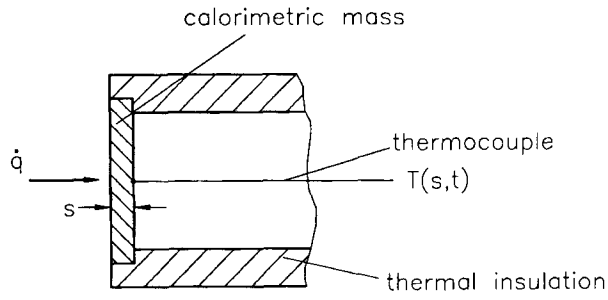

Figure 14. Sketch of slug calorimeter

Again equation (21) is applied for the calculation of the heat flux rate from the measured temperature history on the backside of the disc. The accuracy depends strongly on the quality of the insulation, i.e. prevention of radial heat conduction.

4.3.3 Water cooled calorimeter

The Institute of Mechanical Problems (IPM) in Moscow developed a water cooled calorimeter to measure the heat flux rate in steady state flow conditions [11]. This technique is based on the measurement of the energy absorbed by cooling water, which removes the incident heat from the back surface of the thin metallic disc of a hollow cylinder (**Fig. 15**).

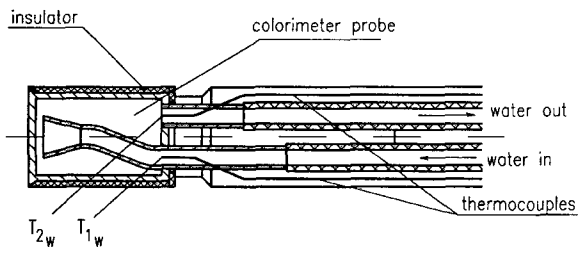

Figure 15. Sketch of water cooled steady state calorimeter

The water mass flow rate and the temperature increase of the water are measured precisely. The heat flux rate is calculated using following relation:

$$\dot{q} = \frac{\dot{m}_c C_{pc} (T_{2c} - T_{1c})}{A} \tag{22}$$

where

A: cross section area of the probe

C_{pc}: specific heat of water

$\dot{m}_c$: water mass flow rate

T_{1c}: water inlet temperature

T_{2c}: water outlet temperature

Material of different catalysis can be used as probe material. DLR and VKI have manufactured calorimeter probes based on IPM-concept (**Fig. 16**).

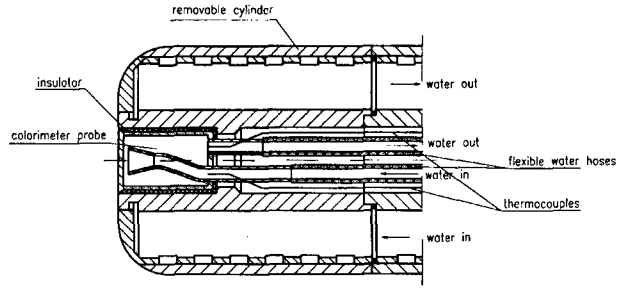

Figure 16. Water cooled calorimeter probe of DLR based on IPM concept

4.4 Heat conduction gauges

4.4.1 Gardon gauge (asymptotic calorimeter)

Gardon gauges consist basically of a thin metallic foil suspended over a cavity in a heat sink. It is thermally and electrically attached to the heat sink at the periphery of the cavity using metallurgical bonding techniques (**Fig. 17**). The metallic foil as

the first thermoelectric material (mostly constantan) creates together with to the second thermoelectric material of periphery (copper) one junction of the thermocouple. A wire of second thermoelectric material is attached to the rear surface center of the foil to form a differential thermocouple. It measures the temperature difference between the center and the edge of the foil.

The one-dimensional heat conduction in radial direction can be described in polar co-ordinates as:

$$\frac{\rho C_p}{K}\frac{\partial T}{\partial t} = \frac{1}{r}\frac{\partial T}{\partial r} + \frac{\partial^2 T}{\partial r^2} + \frac{\dot{q}}{s.K} \qquad (23)$$

with boundary conditions

$$T(r,0) = T_s \quad \text{at} \quad 0 < r < R \qquad (24)$$

and

$$T(R,t) = T_s \quad \text{for} \quad 0 < t < \infty. \qquad (25)$$

The steady state solution of the equation (23) under these boundary conditions is:

$$\dot{q} = \frac{4sK}{(R^2 - r^2)}(T - T_s). \qquad (26)$$

The heat flux rate at the foil center ($r = 0$) would be

$$\dot{q} = \frac{4sK}{R^2}(T - T_s). \qquad (27)$$

Equations (26) and (27) show that the temperature difference between the center and edge of the foil is directly proportional to the heating rate $\dot{q}$. A further thermocouple is usually integrated inside the cylinder to provide absolute gauge temperature for the calculation of heat transfer coefficient in aerodynamic application. The influence of the heat sink temperature should be considered by the specification of the sensor. Copper-Constantan combination meets the requirements with respect to the linearity of the sensor.

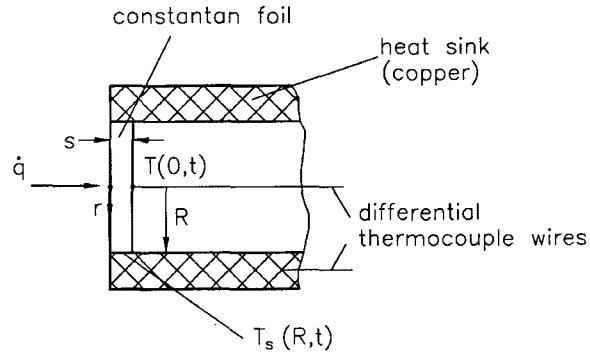

Figure 17. Principle scheme of Gardon gauge

Gardon gauges have a broad application in wind tunnel heat flux measurements and heat transfer determination during flight. Uncooled sensors can only be applied at surface temperatures up to 1100°C. The response time of these sensors is about 1 second. Since the heat flux rate is directly proportional to the temperature difference, the data reduction is very easy. Low sensitivity and limited surface temperature are main disadvantages. Gardon gauge signal in high enthalpy facilities is noisy.

4.4.2 Thin thermopile sensors

The thermopile measurement technique is based on the measurement of the temperature change across the thermal resistance elements, which are deposited on a heat sink material. The thermopile consists of multi thermocouple pairs to achieve measurable voltage drop across the sensor.

Vatell Corporation has developed a micro-sensor (HFM) based on this technique. Two different thin films are deposited on the aluminium nitride substrate of HFM. A thin film of less than 2 microns of the heat flux sensor HFS allows to achieve very fast response of about 10 microseconds. The heat flux sensor is surrounded by a temperature sensor made of platinum resistors (RTS). Temperature is determined by passing a small constant current through the resistance and measuring the resulting voltage. Substrate surface temperature is used to consider the change of the material properties with the temperature in the heat flux determination. It may also be used to check the calibration of the HFM sensor and measure the heat transfer coefficient in aerodynamic application.

In order to use the linear range of the temperature dependency of substrate material properties, the heat transfer to the surrounding model is forced by using nickel or copper housing, which is bonded to the substrate with high grip. The surface of the thin films can be coated with layers of different emissivity, which is very essential for the calibration of the sensor using radiation sensors. HFM sensors can be used at temperatures up to 1125 K without cooling.

In the frame of X-38 programme OHB will use a HFM sensor integrated in a flexible insulation material (FEI) and perform heat flux measurement on the Lee side of the vehicle during the first flight of the X-38 demonstrator (**Fig. 18**) [12].

The OHB set-up including HFM sensor has been qualified at flight conditions of X-38 demonstrator in the arc heated facility LBK of DLR (**Fig. 19**) [13].

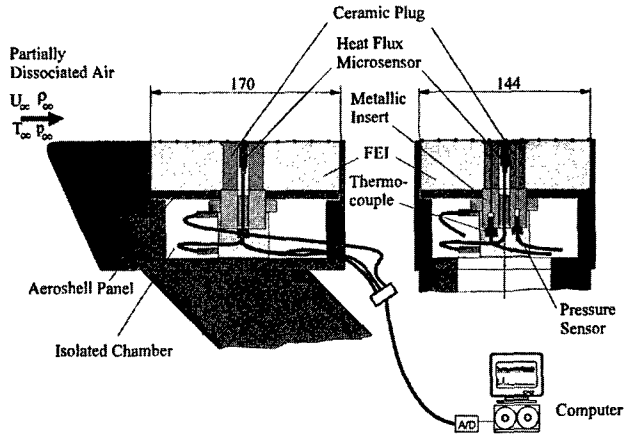

Figure 18. HFM sensor integrated in the OHB flight component [12]

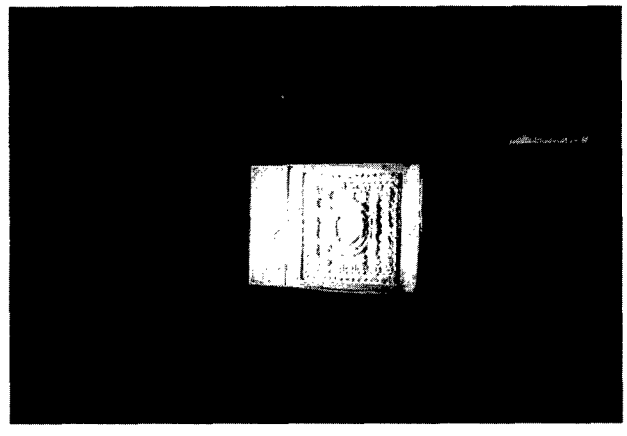

Figure 19. Qualification test on OHB flight component with a HFM sensor in LBK

5. Calibration of heat flux sensors

Calibration of heat flux sensors is a sophisticated work for engineers. Since heat sources based on convective heating is difficult to handle with respect to their repeatability, mostly radiative calibration sources are used. AEDC has developed two such calibration sources. The first source uses a 1.6 kW xenon arc lamp focussed on a small area to achieve high heat flux rates up to 28.4 MW/m^2. To improve the uniformity of the radiant intensity, which is a general problem of most of the radiant heat sources, an integrator consisting of an alu-

minium tube with a highly polished inside surface was installed with its entrance at the focal plane of the calibrator. Another portable calibrator for lower heat flux rate up to 1.4 MW/m^2 has a 200 W tungsten filament lamp as heat source. The radiant energy of the lamp is focussed on a small spot of about 7.6 mm at one of the focal point of the ellipsoidal reflector with polished surface (**Fig. 20**). The sensor is placed at this focal point.

Both calibration techniques require a reference sensor in addition to the sensor, which has to be calibrated.

The calibration unit of Vatell uses the radiation of a electrically heated thin graphite plate as heat source [12]. The reference and calibration sensor are installed at each sides of the plate and heated with same radiance intensity. In order to avoid any convection and oxidation processes, the complete furnace is set evacuated down to 1 hPa pressure level. Heat flux rate up to 3.4 MW/m^2 can be achieved in this heat flux calibration source.

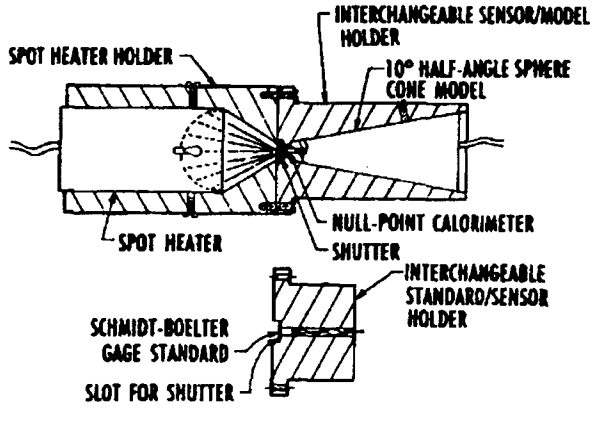

Figure 20. Sketch of portable calibrator of AEDC [8]

6. Comparative heat flux measurements in LBK

Transient heat flux probe and water cooled steady state calorimeter of LBK (Figs. 4 and 16) are used for the measurement of cold wall heat flux rate to a copper surface at same test conditions. Tests were performed in the stagnation point test configuration of LBK. Both flow conditions were chosen in such a way that moderate heat flux rates can be set. A SiC model with the same geometry as heat flux probes was also tested to determine the hot wall heat flux rate. The duration of the tests on the SiC probe was long enough to reach radiative equilibrium. As mentioned before the hot wall heat flux is determined from the measured surface temperature with a pyrometer. Measured cold and hot wall heat flux rates are listed in **Table 1**.

Test condition	**I**	**II**
$\dot{q}_{c,t}$ [kW/m^2]	725	1080
$\dot{q}_{c,s}$ [kW/m^2]	680	1210
$\dot{q}_h$ [kW/m^2]	303	351

Table 1. Cold wall heat flux rates to a copper surface measured using transient and calorimeter probes in comparison with hot wall heat flux rates to a SiC model in LBK

Although at test condition I the agreement between cold wall heat flux rates measured with the transient and calorimeter probes ($\dot{q}_{c,t}$ and $\dot{q}_{c,s}$, respectively) is acceptable, a deviation of around 11% is noticed at the test condition II. A systematic study including a detailed parameter variation is underway to clarify this discrepancy. Another very important results, which is strongly related to non-

equilibrium effects of high enthalpy flow on model surfaces with different catalycity, is the difference between cold and hot wall heat flux rates. As it can be seen in the Table 1 the cold wall heat flux rate is more than twice of the hot one. Since the gas temperature at the stagnation point in the boundary layer flow of the model of more than 4000 K is remarkably higher than the model surface temperature and the difference in the surface temperature of SiC and copper cylinder of cold wall heat flux probes is about 1500 K, this big difference has to be caused by additional gas surface interaction effects. At temperatures beyond 2500 K molecular oxygen in the flow field of LBK is completely dissociated. Spectroscopic measurements and numerical results state that the flow field in the free stream and behind bow shock ahead of the model is in thermochemical non-equilibrium (nearly frozen). Therefore the surface catalysis has an significant influence on the heat flux rate. It is well known that at above specified test condition a SiO_2 layer develops due to passive oxidation on the SiC surface. This leads to a low catalytic surface. In contrary copper surface is nearly fully catalytic. Therefore strong exothermic recombination reaction takes place on the copper surface and enhance the heat flux rate. Especially non-equilibrium effects on the gas surface interaction keeps heat flux measurements in high enthalpy flow fields very challenging and require further improvements.

7. Concluding remarks

Parallel to the progress in material science, electronics, and spectroscopic techniques the accuracy and application range of heat flux sensors has been improved in the last decades. But compared to other parameters in aerothermodynamics like pressure, flow rate, etc., where accuracy and repeatability values are specified within 1%, usually an accuracy value within 5% cannot be guaranteed for heat flux sensors, yet. Another challenge for engineers is the development of sensors of high accuracy for high temperature application in a reactive environment.

8. References

[1] Fay, J. A.; Ridell, F. R.; *Theory of Stagnation Point Heat Transfer in Dissociated Air.* Journal of Aeronautical Sciences, vol. 25, no. 2, pp. 73-85, February 1958.

[2] Andreson, J. D.; *Hypersonic and High Temperature Gas Dynamics.* McGraw-Hill Inc., 1989.

[3] Dorrance, W. H.; *Viscous Hypersonic Flow.* McGraw-Hill Inc., 1962.

[4] Kindler, K.; *Ermittlung einer zeitlich veränderlichen Wärmebelastung auf einen endlichen Zylinder.* 5. Jahrestagung der DGLR in Berlin, Vortrag Nr. 72, 1972.

[5] Grönig, H.; *Kurzzeitmeßtechnik.* Vorlesungsmanuskript der RWTH Aachen.

[6] Fujii, K.; *Thermal Model of the Sensor Plug and Derivation of Heat Transfer Rate from TC Temperature.* TN of NAL, Tokyo, 1996.

[7] Inouye, Y. et.al.; *Quick Report of HYFLEX Onboard Measurements.* 20th International Symposium on Space Technology and Science, Gifu, Japan, May 19-25, 1996.

[8] Kidd, C. T.; *Recent Developments in High Heat-Flux Measurement Techniques at the AEDC.* ISA Paper No. 90-156, presentation at 36th ISA International Instrumentation Symposium, Denver, Col., pp. 477-492, May 1990.

[9] Olivier, H; Grönig, H.; *Instrumentation Techniques of the Aachen Shock Tunnel TH2.* Paper at International Congress on Instrumentation in Aerospace Simulation Facilities (ICIASF), Ohio, USA, 1995.

[10] Jessen, C; Grönig, H.; *A new method for manufacture of thin film heat flux gauges.* Shock Waves, 1, 161-164, Springer Verlag, 1991.

[11] Yakushin, M. I.; *Test Report on Oxidation Tests in IPG-Facility.* IPM RAS, Moscow, April 1995.

[12] Janovsky, R.; Tausche, M.; Romberg, O.; *A Contribution to the Aerothermodynamic Measurement System of the X-38.* Proceedings of the International Symposium on Atmospheric Reentry Vehicles and Systems, Arcachon, March 1999.

[13] Gülhan, A.; Esser, B.; *Qualification Tests on the OHB Aerothermodynamic Measurement System in the Arc Heated Facility LBK.* TET-DLR-21-TN-3401, May 1999.